PHYSICAL REVIEW B VOLUME 59, NUMBER 6 1 FEBRUARY 1999-II

Orbital polarization in $NiFe_2O_4$ measured by Ni-2p x-ray magnetic circular dichroism

G. van der Laan
Daresbury Laboratory, Warrington WA4 4AD, United Kingdom
and Department of Physics, University of York, York YO1 5DD, United Kingdom

C. M. B. Henderson and R. A. D. Pattrick
Daresbury Laboratory, Warrington WA4 4AD, United Kingdom
and Department of Earth Science, University of Manchester, Manchester M13 9PL, United Kingdom

S. S. Dhesi
Daresbury Laboratory, Warrington WA4 4AD, United Kingdom
and Department of Physics, University of York, York YO1 5DD, United Kingdom

P. F. Schofield
Department of Mineralogy, Natural History Museum, London SW7 5BD, United Kingdom

E. Dudzik
Daresbury Laboratory, Warrington WA4 4AD, United Kingdom
and Department of Physics, University of York, York YO1 5DD, United Kingdom

D. J. Vaughan
Department of Earth Science, University of Manchester, Manchester M13 9PL, United Kingdom

(Received 3 August 1998)

We report a comprehensive study of the x-ray magnetic circular dichroism (XMCD) at the Ni $L_{2,3}$ edges of $NiFe_2O_4$ (trevorite), a ferrimagnetic compound which belongs to the class of strongly correlated $3d$ systems. The measured XMCD line shape is in good agreement with full-multiplet calculations for a $3d^8$ ground state including an octahedral crystal field of $10Dq = 1.2$ eV. Using the XMCD sum rules, we find for the nickel an orbital to spin magnetic moment ratio of $L/S = 0.27 \pm 0.07$, which means that the orbital contribution to the magnetic moment is $12 \pm 2\,\%$. The size of the error bar is not due to the neglect of band structure and hybridization, but due to Coster-Kronig transitions which give a transfer of spectral weight in the dichroism near the L_2 edge. Using the sum rules for the isotropic x-ray absorption spectrum, we obtain the expectation value of the spin-orbit interaction, which can be converted into an L/S ratio of 0.34 ± 0.11. All sum-rule results were corrected for the influence of core-valence exchange interaction, which gives rise to *jj* mixing between the two absorption edges. The correction is done by comparing the calculated sum-rule results with the correct ground-state values calculated as a function of crystal-field strength. The 2-eV shoulder of the L_3 line shows a strong positive dichroism, which can be attributed to a spin-flip state. From the overall agreement between the experimental and theoretical results, we conclude that a localized model provides a good description for the orbital magnetization. [S0163-1829(99)12005-8]

I. INTRODUCTION

In the last few years there has been a surge of interest in the use of circularly polarized x rays to study the electronic and magnetic structure of magnetically ordered systems. X-ray magnetic circular dichroism (XMCD) has been established as a powerful, element-selective tool to separate the spin and orbital contributions to the total magnetic moment. Whereas the majority of XMCD studies was performed on ferromagnetic metals,[1,2] there have been relatively few measurements on metal oxides[3–6] despite the fact that the theoretical spectra for these localized materials were already available since the early development of this technique.[7]

The electronic structure of heavy $3d$ transition-metal monoxides has been a controversial subject ever since the discovery of their insulating properties,[8] which are in sharp contrast with one-electron band-structure theory which predicts metallic behavior.[9–11] This insulating behavior is believed to be due to strong electron correlation effects, which make the one-electron model inapplicable. According to the Mott-Hubbard model,[12,13] the large on-site d-d Coulomb repulsion U suppresses high-energy charge fluctuations, which describe the hopping of a d electron between two metal sites. Although the Mott-Hubbard model explains the existence of a wide optical gap, it fails to predict the size of the optical gap[14] as well as the x-ray spectra of $3d$ transition-metal oxides, halides, and chalocogenides.[15] The optical gap in these materials is determined by the charge-transfer energy Δ, which is the energy required to transfer an electron from a ligand to a metal site, i.e., $d^n \rightarrow d^{n+1}\underline{L}$, where $\underline{L}$ denotes a hole in the ligand band.[16] NiO was originally believed to be a Mott-Hubbard insulator, i.e., with the gap determined by

U, but Fujimori and Minami[17] showed by using a cluster model for the valence-band photoemission that this material is actually a charge-transfer insulator. The combination of photoemission and inverse photoemission data gives an experimental value for the band gap of 4.3 eV,[18,19] while density functional theory predicts a gap of only 0.3 eV.[20]

The orbital polarization in $3d$ transition-metal oxides has been recognized for a long time, e.g., in the interpretation of the magnetic susceptibility[21] and magnetic neutron scattering.[22] However, electronic structure calculations, such as augmented-spherical-wave,[20] Hartree-Fock,[23] and cluster model[24] calculations, often neglect the spin-orbit interaction in these oxides. This results in an absence of orbital polarization and consequently a wrong description of magnetic properties such as the magnetocrystalline anisotropy[25,26] and magnetorestriction.[27] Taking spin-orbit coupling into account, Svane and Gunnarsson[28] calculated an orbital to spin magnetic moment ratio L/S of 0.35 for NiO using the self-interaction-corrected local-spin-density approximation (SIC LSDA). This value was recently confirmed by Fernandez *et al.*[29] who measured an L/S ratio of 0.34 ± 0.06 using magnetic x-ray scattering. Of course, the good agreement between the calculations and experimental results can be fortuitous. The absence of a concept for the electric current in the LSDA is known to underestimate the size of the orbital moment, which can cause serious problems in systems with large orbital moments, such as rare-earth and actinide structures.[30] Recent developments made using the so-called LDA$+U$ approach have led to improved results.[31] The study of $3d$ transition-metal oxides remains, therefore, of considerable interest. In this paper, we report on the orbital polarization in $NiFe_2O_4$ using XMCD, which permits an element-selective separation of the spin and orbital contributions to the total magnetic moment. This technique can be applied to ferro- and ferrimagnets, but not to antiferromagnets, which have no net magnetization. This makes it attractive to study $NiFe_2O_4$ (trevorite), where the Ni^{2+} ions in octahedral coordination are aligned ferromagnetic with respect to each other. The crystal structure of $NiFe_2O_4$ is identical to that of Fe_3O_4 (magnetite), which has an inverse spinel structure consisting of two iron magnetic sublattices which are antiferromagnetically coupled by superexchange through the oxygen ions. One magnetic sublattice contains 1/3 of the iron atoms as Fe^{3+} in tetrahedral sites, while the other magnetic sublattice contains the remaining 2/3 iron atoms in octahedral sites as both Fe^{3+} and Fe^{2+} ions. In trevorite, the Fe^{2+} ions in the octahedral sites of magnetite are replaced by Ni^{2+}.

In this study we compare the measured Ni $2p$ x-ray absorption spectroscopy (XAS) and XMCD of trevorite with calculated spectra using a crystal-field model including multiplet structure. As predicted in Refs. 32 and 33, there is a strong dependence of the orbital moment on the crystal-field strength. We relate the localized electronic structure of divalent Ni compounds to the spectral features in the Ni $2p$ XAS. This reveals that the ground state has mainly e_g^2 character, where the orbital moment is induced by second-order spin-orbit interaction. We determine the orbital polarization using three different approaches: (i) by detailed comparison of the experimental spectrum with the calculated line shape, (ii) by using the sum rules for the XMCD spectrum, and (iii) by using the sum rules for the XAS spectrum. After correcting the sum-rule results for the effects of jj mixing, we find an orbital magnetization which is in good accordance with the XMCD line shape predicted by the crystal-field model.

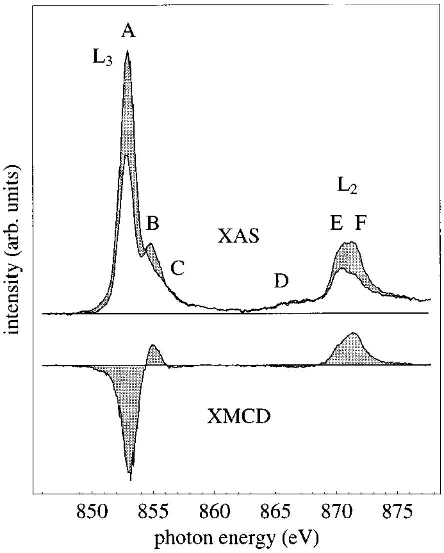

FIG. 1. Measured Ni $L_{2,3}$ absorption spectra of $NiFe_2O_4$ for parallel and antiparallel alignment of the light helicity and magnetization direction, together with the difference spectrum, the XMCD. Labels $A-F$ are explained in the text.

II. EXPERIMENTAL RESULTS

$NiFe_2O_4$ was synthesized by heating a stoichiometric mixture of Fe_2O_3 and NiO in a muffle furnace at 1100 °C for 3 days. Sample purity was confirmed by x-ray powder diffraction, which revealed a cell parameter of 8.340(1) Å. In the XAS measurements we used a pressed pellet containing a 50% mixture of finely ground (micron size) $NiFe_2O_4$ and high-purity graphite, to increase the conductivity.

XAS was performed on the high-energy spherical grating monochromator beam line 1.1 of the Synchrotron Radiation Source at Daresbury Laboratory using 75% circularly polarized x rays. The energy scale was calibrated using the Ni L_3 edge of NiO.[34] The sample was mounted onto a rod inside a small vacuum chamber (10^{-7} torr) contained between the coils of a superconducting magnet. The sample magnetization was along the direction of x-ray beam, i.e., along the light helicity vector. The absorption signal was recorded in drain current mode and normalized to the incident x-ray flux. XMCD spectra were obtained by taking the difference spectrum between scans with opposite magnetization of ±2 T at room temperature. Although the counting statistics was reduced by the poor electric conductivity of the trevorite, the spectra were completely reproducible in repeated scans.

Figure 1 shows the Ni $2p$ XAS spectra of trevorite for parallel and antiparallel alignment of the light helicity vector and magnetization direction. Reversal of the magnetization has the same effect as reversal of the light helicity vector. When the magnetization is along the positive z axis, the parallel and antiparallel alignment can be denoted by right circularly polarized (rcp) and left circularly polarized (lcp) light, respectively. The L_3 peak height increases by 65% for antiparallel compared to parallel alignment. The shoulder B is only observed for parallel alignment. The L_2 edge is roughly split into two peaks which reverse in height for opposite magnetizations. The bottom curve shows the difference spectrum for parallel minus antiparallel alignment, the XMCD. The L_3 edge shows the peak *A* at a photon energy of 853 eV with negative dichroism, the shoulder *B* at 2 eV higher energy with positive dichroism, and the weak feature *C* at 4 eV higher energy with negative dichroism. The two discernible peaks *E* and *F* in the L_2 structure have positive dichroism. There is a gradual increase in the ''background'' from 863 eV onwards, labeled *D* in Fig. 1, which shows a negative dichroism.

III. LOCAL ELECTRONIC STRUCTURE

As a result of the dipole selection rules, the $2p$ XAS spectrum reflects directly the nature of the $3d$ electronic ground state. In order to make an assignment of the peak structures in divalent Ni compounds, we follow the analysis presented in Ref. 34 using the framework of the Anderson impurity model including full-multiplet structure. Related treatments can also be found in Refs. 35–38. The local ground state is a mixture of the configurations d^8, $d^9\underline{L}^2$, and is determined by the d-L charge-transfer energy Δ, the d-d Coulomb interaction, U, and the d-L mixing (hybridization). The final state in XAS, where an electron has been excited from a $2p$ core level into an empty $3d$ state, is a mixture of the configurations $\underline{2p}3d^9$ and $\underline{2p}3d^{10}\underline{L}$. The $2p$-$3d$ exchange interaction gives a multiplet structure for the $\underline{2p}3d^9$ configuration, whereas the bandlike character of the ligand hole results in a broad feature for the $\underline{2p}3d^{10}\underline{L}$ configuration. Hybridization mixes the two configurations, which results effectively in a reduced multiplet width for the $\underline{2p}_{3/2}3d^9$ final state. This can also be interpreted as a reduction of the $2p$-$3d$ exchange interaction due to the delocalization of the valence hole. The prominent features *A*, *B*, *C*, *E*, and *F* in Fig. 1 can be ascribed to the multiplet structure of a final state with mainly $\underline{2p}3d^9$ character, where the large spin-orbit interaction of the core level splits the spectrum into a $2p_{1/2}$ (L_2) and $2p_{3/2}$ (L_3) manifold with an energy separation of 17 eV. The peak separation *A*-*B* is a measure for the reduction factor of the $\underline{2p}_{3/2}3d^9$ multiplet structure and can therefore be used as a ''ruler'' for the covalency of the nickel.[34] The 2-eV peak splitting in trevorite is close to the value of 1.9 eV reported for NiO_2,[34,39,40] which has $\Delta = 4.6$ eV and a ground state of 73% d^8 character with the rest mainly d^9 character. The $\underline{2p}3d^{10}\underline{L}$ final state is expected to be located at ~5 eV above the $\underline{2p}3d^9$ state.[34] Unlike NiO and nickel dihalides, which show weak features that can be assigned to the broadened ligand final states, the spectrum of trevorite does not reveal the presence of these states. It is, therefore, not meaningful to include the corresponding configurations in a cluster calculation, which would only give additional parameters that cannot be determined properly. Therefore, we assume in the treatment of the spectra that the ground state is completely $3d^8$ and that the final state is $\underline{2p}3d^9$ with a reduced multiplet structure. Such a single-configuration model offers a transparent analysis because the only parameters are the octahedral crystal-field strength, $10Dq$, and the scaling factor κ of the Slater integrals.

We now turn to the explanation of the structure *D* in Fig. 1. The sudden creation of the $2p$ core hole in XAS can induce and excitation of an electron from the ligand band into the continuum state k above the ionization threshold.[41] Also, in nickel dihalides the onset of an increase in the ''background'' around 10 eV above the main line has been ascribed to this type of excitation, where the final state can be assigned to a mixture of $\underline{2p}_{3/2}3d^9\underline{L}k$, $\underline{2p}_{3/2}3d^{10}\underline{L}k$, and $\underline{2p}_{3/2}3d^8k$ configurations.[34]

IV. SPIN-FLIP STATE

Whereas the XAS spectrum reflects the local electronic structure, the XMCD contains specific information about the alignment of the spin and orbital moments in the final states. Analysis of the XMCD provides therefore a deeper insight in the excitation process.

The initial state of Ni^{2+} contains two empty d states of spin-down character. Peak *A* in the Ni $2p$ XAS spectrum is due to the transition of a spin-down core electron into one of the empty d states under spin conservation. The final state with the spin-down core and valence holes is a triplet state. Peak *B* is due to the transition of a spin-up core electron into an empty spin-down d state. This gives a single final state, which is shifted towards higher energy by the effective $2p$-$3d$ exchange interaction. This spin-flip transition becomes allowed when the selection rule $\Delta S = 0$ is broken by the strong $2p$ spin-orbit interaction. Further evidence for the spin-flip state can be obtained from the XMCD spectrum. This becomes clear if we visualize the $2p$ absorption process as a two-step model. The core level is split into $j = 3/2$ and 1/2 states where spin and orbit are coupled parallel and antiparallel, respectively. In the first step, the emission with parallel and antiparallel alignment of light helicity and magnetization results in photoelectrons of preferred spin-up and spin-down directions, respectively. In the second step, these photoelectrons have to find their place in the valence band. If there are only spin-down holes available, the XMCD spectrum will show a negative L_3 and a positive L_2 peak. Because the exchange interaction couples the spin of the core hole to that of the valence electrons, the core-hole states with spin down and spin up are at the low- and high-energy sides of each edge, respectively. Since in the L_3 edge the spin and orbit are coupled parallel, the spin-down core hole (triplet final state) gives a negative dichroism, while the spin-up core hole (singlet final state) gives a positive dichroism. The sign of the XMCD in Fig. 1 confirms that peaks *A* and *B* correspond to a triplet and singlet state, respectively. In the L_2 edge the spin states are less pure so that the effect is less pronounced.[42] As an additional advantage, the XMCD spectrum offers an accurate way to determine the reduction factor of the core-valence exchange interaction.

V. ORBITAL MAGNETIZATION OF CRYSTAL-FIELD STATES

The orbital magnetization depends on the subtle interplay between spin-orbit and crystal-field interaction. An octahedral crystal field splits the d states into t_{2g} states (*xy*, *yz*, and *zx* orbitals) and e_g states (x^2-y^2 and $3z^2-r^2$ orbitals) with an energy separation $10Dq$. The two degenerate e_g states have the highest energy and contain two holes with spins parallel in order to maximize the exchange energy.

Thus the d^8 ground state is $(e_g^2\,{}^3A_2)T_2$, where A_2 denotes the irreducible representation of the orbital state in the octahedral symmetry group and T_2 denotes the irreducible representation of the spin-orbit coupled state in the octahedral double group. The pure $e_g^2\,{}^3A_2$ ground state is nondegenerate so that the orbital moment vanishes. This is sometimes put forward as an argument that the orbital magnetism in divalent nickel compounds can be neglected. However, as we will show below this can not be justified.

An electron in a specific orbital state has an angular momentum along a given axis when, by rotation about that axis, the orbital can be transformed into an equivalent and degenerate orbital which does not contain an electron with the same spin.[43] Such a transformation will allow the electron cloud to rotate about the axis; i.e., there is an orbital moment along that axis. For instance, a rotation of 45° about the z axis will turn the xy orbital into the x^2-y^2 orbital, whereas a rotation of 90° changes the xy orbital into the yz orbital. Thus one expects an orbital moment from an electron in either of these pairs of orbitals. The $3z^2-r^2$ orbital cannot be transformed into any of the other orbitals by a rotation about the z axis; thus, it will not give an orbital moment in the z direction. The octahedral crystal field removes the degeneracy of the xy and x^2-y^2 orbitals and, in second order, i.e., $\zeta \ll 10Dq$, the orbital contribution is reduced by a factor proportional to $\zeta/10Dq$. Because the $3z^2-r^2$ and x^2-y^2 orbitals cannot be transformed into each other by rotation about any axis, the e_g representation has no orbital moment. However, there is an orbital moment due to second-order spin-orbit interaction which mixes $(e_g t_{2g}\,{}^3T_2)T_2$ and $(e_g t_{2g}\,{}^1T_2)T_2$ into the ground state with coefficients $\sqrt{2}\zeta/10Dq$ and $\zeta/(10Dq+8F_2+30F_4)$, respectively. In the following we will use the full diagonalization of the Hamiltonian to take into account the orbital magnetization.

VI. MULTIPLET CALCULATIONS

Ground-state properties and x-ray spectra were calculated at $T=0$ an intermediate coupling using Cowan's *ab initio* Hartree-Fock code with relativistic correction.[44] For the Ni $3d^8$ configuration, the spin-orbit interaction is $\zeta \equiv \zeta(d) = 0.083$ eV and the Slater integrals are $F^2(d,d)=12.234$ eV, $F^4(d,d)=7.598$ eV, and for the Ni $2\underline{p}3d^9$ configuration $\zeta(2p)=11.507$ eV, $\zeta(d)=0.102$ eV, $F^2(p,d)=7.721$ eV, $G^1(p,d)=5.787$ eV, and $G^3(p,d)=3.291$ eV. Interatomic screening and mixing with the $2\underline{p}3d^{10}\underline{L}$ final state (cf. Sec. III) are taken into account by reducing the Slater integrals with a factor κ. The spin-orbit parameters were not reduced. An exchange field of $\mu_B H=0.01$ eV was applied along the positive z axis. The crystal field was included using the chain of group method.[45]

Figure 2 shows the calculated XAS and XMCD spectra for different values of $10Dq$. The spectra exhibit strong changes when $10Dq$ is of the order of ζ. Around $10Dq = 0.15$ eV the spin of the L_2 edge in the XMCD spectrum changes from negative to positive. At $10Dq=0.4$ eV the shoulder B of the L_3 edge reverses in sign. For $10Dq$ larger than 1 eV, the line shape remains essentially the same, because the $2\underline{p}_{3/2}e_g$ final state [marked by the arrow in Fig. 2(a)] is then well separated in energy from the $2\underline{p}_{3/2}t_{2g}$ final state, which has only a small transition probability. The splitting of the L_2 and L_3 edges into the doublet structures A-B and D-E does not depend on $10Dq$, but scales with κ, the reduction factor of the $2p$-$3d$ exchange interaction. The energy separation A-B of 2 eV fixes the value of κ to 0.8. The intensity ratios A:B and E:F in the XMCD depend on both κ and $10Dq$, because both parameters influence the spin mixing in the final state. Thus these intensity ratios provide, together with the L_3:L_2 ratio, a sensitive measure for $10Dq$.

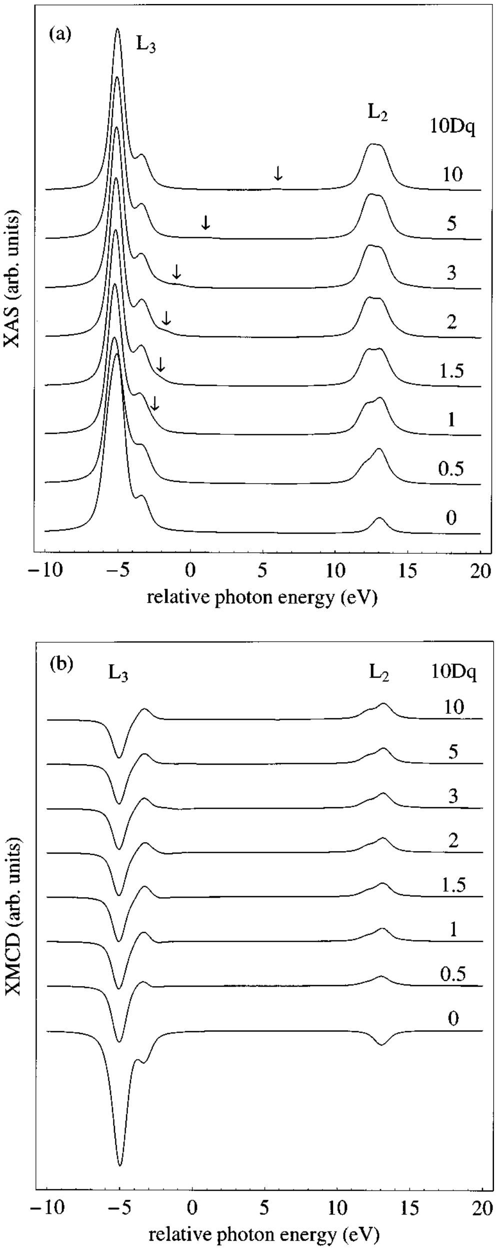

FIG. 2. Calculated Ni $L_{2,3}$ XAS (a) and XMCD (b) spectra for a $3d^8$ ground state with different octahedral crystal-field strength $10Dq$. The arrows in the XAS spectra mark the energy position of the $2\underline{p}_{3/2}t_{2g}$ final state. The spectra were convoluted with a Lorentzian of $\Gamma=0.3$ (0.4) eV for the L_3 (L_2) absorption edge to account for intrinsic linewidth broadening and a Gaussian of $\sigma=0.4$ eV for instrumental broadening.

Figure 3 shows the theoretical result for $10Dq=1.2$ eV, which gives the best agreement with the measured XMCD. The calculations include a Lorentzian of $\Gamma=0.3$ (0.4) eV for

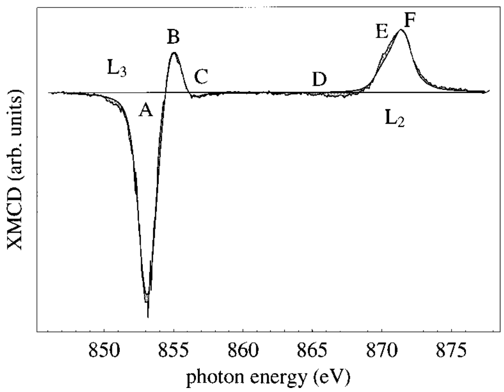

FIG. 3. Comparison between the measured Ni $2p$ XMCD of $NiFe_2O_4$ and the calculated signal for a d^8 ground state with $10Dq=1.2$ eV. The spectra were convoluted with a Lorentzian of $\Gamma=0.3$ (0.4) eV for the L_3 (L_2) absorption edge to account for intrinsic linewidth broadening and a Gaussian of $\sigma=0.5$ eV for instrumental broadening.

the L_3 (L_2) edge to account for intrinsic linewidth broadening and a Gaussian of $\sigma=0.5$ eV for instrumental broadening. It is clear that the agreement for the L_3 edge is almost perfect. In the L_2 edge, the calculated dichroism of the peak E is smaller than that of the measurement. This effect is compensated by a negative dichroism in the region labeled D. This transfer of spectral weight can be ascribed to a Coster-Kronig interaction $R(2p_{3/2},k;2p_{1/2},3d)$ between the discrete states $\underline{2p}_{1/2}3d^9$ and continuum states $\underline{2p}_{3/2}3d^8k$. Such an effect was not included in the calculation. Because the spin and orbit of the $2p_{3/2}$ core hole are coupled parallel, the dichroism in the region D is expected to be negative, which is in agreement with the experimental observation.

The feature C, which is barely discernible in the isotropic spectrum, but quite prominent in the dichroism, corresponds to a final state $\underline{2p}_{3/2}t_{2g}$ [cf. Fig. 2(a)]. Finally, we mention that within the limits of the counting statistics, there is no evidence for any structure from a $2p_{3/2}3d^{10}\underline{L}$ final state. In the XAS of NiO and nickel dihalides, these structures are found in the region between C and D.

VII. SUM-RULE RESULTS

The most obvious trend in the XAS and XMCD spectra of Fig. 2 is the change of the $L_{2,3}$ areas, which can be related to a reduction of the ground-state moments as a function of $10Dq$. Such a relation is straightforward to derive in the case of the orbital moment.[46] The light acts only on the orbital part of the wave function, and the dependence on the spin arises from the spin-orbit interaction. The selection rules for electric dipole transitions are $q\equiv-\Delta m=+1$, 0, and -1 for rcp, z perpendicular, and lcp light, respectively. The total intensity is obtained by integrating over all magnetic sublevels of the core level. This yields an expression for the transition probability which contains only the polarizations of the ground state and light. For q polarized light, the intensity integrated over the core level can be written in terms of m and q as

$$\rho_q=\sum_m \langle n_m\rangle\left[\frac{1}{3}+\frac{qm}{2l}+O(q^2,m^2)\right], \tag{1}$$

where $\langle n_m\rangle$ is the occupation number of the holes in the sublevel m of the valence shell l. The quadratic term has not been written out explicitly, but can be found elsewhere.[47] This term relates the integrated linear dichroism to the quadrupole moment. However, as we will show below, the quadrupole moment vanishes in octahedral crystal field. Summation over q gives

$$\rho_{\text{iso}}\equiv\rho_1+\rho_0+\rho_{-1}=\sum_m \langle n_m\rangle\equiv n, \tag{2}$$

which shows that the integrated signal of the isotopic spectrum is proportional to the total number of holes, n, in the l shell. ρ_0 can only be measured when the geometry is changed, instead one normally uses the sum spectrum

$$\rho_{\text{sum}}=\rho_1+\rho_{-1}\approx\tfrac{2}{3}\rho_{\text{iso}}, \tag{3}$$

which is only correct in the absence of linear dichroism.

The integrated XMCD spectrum

$$\rho_{\text{XMCD}}\equiv\rho_1-\rho_{-1}=l^{-1}\sum_m \langle n_m\rangle m\equiv l^{-1}\langle L_z\rangle \tag{4}$$

is proportional to the expectation value of the orbital moment, L_z. Combining Eqs. (2)–(4), the orbital moment per d hole ($l=2$) is obtained as

$$\frac{\langle L_z\rangle}{n}=\frac{4}{3}\,\frac{\rho_{\text{XMCD}}}{\rho_{\text{sum}}}. \tag{5}$$

We further require sum rules for the spin-dependent operators.[48] Defining the weighted difference over the two integrated absorption edge signals,

$$\delta\equiv\rho(L_3)-2\rho(L_2), \tag{6}$$

the effective spin moment per hole is given as

$$\frac{\langle S_z^{\text{eff}}\rangle^*}{n}=\frac{\langle S_z\rangle^*+\frac{7}{2}\langle T_z\rangle^*}{n}=\frac{\delta_{\text{XMCD}}}{\rho_{\text{sum}}}, \tag{7}$$

where T_z is the magnetic dipole term.[48] The angularly dependent part of the spin-orbit interaction per hole is obtained from the sum spectrum as[49]

$$\frac{\langle l\cdot s\rangle^*}{n}=\frac{\delta_{\text{sum}}}{\rho_{\text{sum}}}. \tag{8}$$

The asterisk indicates that the expectation value of the operator has been obtained from the sum rule. This is not necessarily equal to the correct ground-state value. The sum rules in Eqs. (7) and (8) are no longer exact in the presence of $2p$-$3d$ electrostatic interaction, which gives a transfer of spectral weight between the L_3 and L_2 edges. This effect is called jj mixing.[49] It does not influence L_z because ρ in Eq. (5) is independent of jj mixing. However, the effective spin moment and spin-orbit interaction are proportional to δ, so that they are sensitive to jj mixing.

Using the integrated intensities of the absorption spectra in Fig. 1, corrected for the incomplete polarization of the x rays, the sum rules give the magnetic moments as $\langle S_z\rangle^*=0.35\mu_B$ and $\langle L_z\rangle^*=0.10\mu_B$ per hole. This amounts to a total magnetic moment of $\langle L_z\rangle^*+2\langle S_z\rangle^*=0.80\mu_B$ per hole.

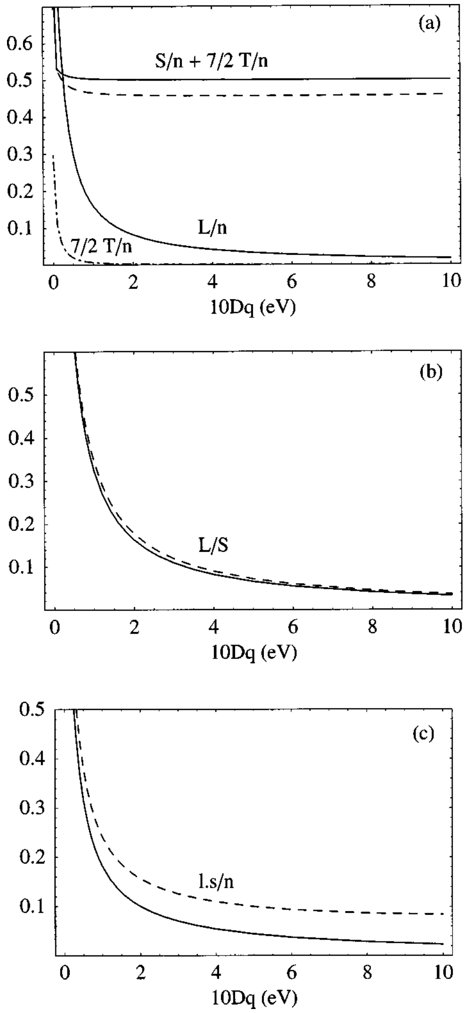

FIG. 4. Expectation values for a $3d^8$ ground state as a function of $10Dq$ obtained by applying the sum rules to the calculated $2p$ XMCD spectra (dotted line) together with the correct ground-state values (solid line). (a) Orbital and spin moments per hole and magnetic dipole term per hole (dash-dotted line), (b) L/S ratio, and (c) spin-orbit interaction per hole.

For $10Dq>1$ eV, the calculation predicts a value of $\langle S_z\rangle^* = 0.45\mu_B$ per hole [cf. Fig. 4(a)], which is thus higher than the measured value. However, the measured magnetic moment merely represents its average value. It can be lowered by the presence of noncollinear moments, incomplete magnetization, or a surface layer which is not ferro- or ferrimagnetic. A further complication arises from the normalization per hole. The signal must be integrated over the entire adsorption edge. This works nicely for the dichroic signal, which goes to zero above the edge when the continuum states become nonmagnetic. However, in the sum spectrum it is less straightforward to separate the discrete states from the continuum states. Figure 1 shows that the ''background'' of the sum spectrum does not have the same height below and above the edges. The normalization using the sum spectrum can be avoided by taking the L/S ratio, in which case the number of holes drops out. We thus obtain an L/S^* of 0.29 ± 0.07. This still needs to be corrected for *jj* mixing, where the precise correction depends on $10Dq$.

Figure 4 shows the calculated moments for a $3d^8$ ground state as a function of $10Dq$. The drawn lines give the moments calculated directly for the ground state. The dotted lines give the moments obtained by applying the sum rules to the calculated $2p$ XMCD spectra. All curves in Fig. 4 show a similar trend, namely, a strong asymptotic descent from the atomic value towards a constant value, which is equal to zero except for the spin moment. The strong enhancement in S_z^{eff} for small $10Dq$ is due to the contribution of T_z. Figure 4(a) shows that T_z (dash-dotted line) increases strongly when $10Dq$ is small compared to ζ. For large $10Dq$ the influence of T_z can be neglected. Its value vanishes in octahedral symmetry, e.g., for $10Dq=1$ eV the value of $\frac{7}{2}T_z/S_z$ is 0.014. A further difference between S_z^{eff} and $S_z^{\mathrm{eff}*}$ arises for small $10Dq/\zeta$ because we used the sum spectrum instead of the isotropic spectrum in the sum rule of Eq. (7). This gives a discrepancy when the linear dichroism is not zero, i.e., when there is a quadrupole moment in the ground state.

With the aid of Fig. 4 we are now able to correct the measured L/S ratio for the effect of *jj* mixing. The result of the sum rule, which was $L/S^*=0.29\pm 0.07$, gives with Fig. 4(a) a corrected value of $L/S=0.27\pm 0.07$. Thus the orbital moment amounts to 12 ± 2 % of the total magnetic moment. The sum-rule result can be compared with the fit to the XMCD line shape for $10Dq=1.2$ eV, which was presented in Fig. 3. This fit corresponds to a d^8 ground state with $L/S=0.27$. The perfect accordance with the L/S value from the sum rule is not accidental. It occurs necessarily because of the constraints on the $L_{2,3}$ areas in the fit.

Another approach to assess the orbital magnetization is to determine the expectation value of the spin-orbit interaction from the areas of the sum spectrum and then to convert this into a value of L/S. Using Eq. (8), we obtain from the areas in Fig. 1 the value of $\langle l\cdot s\rangle^*/n = 0.25\pm 0.08$, which corrected for *jj* mixing [cf. Fig. 4(c)] becomes $\langle l\cdot s\rangle/n = 0.19\pm 0.06$. Using simple arguments, one might guess that, for a more than half-filled shell, the orbital moment per hole is equal to the spin-orbit interaction per spin, i.e., $\langle L_z\rangle/n \approx \langle l\cdot s\rangle/\langle S_z\rangle$. However, the neglect of spin-orbit correlations, other than the diagonal terms, can easily lead to a mismatch of a factor of 2 or more. Therefore, it is better to resort to Fig. 4, from which we find that the obtained $\langle l\cdot s\rangle/n$ value corresponds to a $10Dq$ value between 0.7 and 1.4 eV and an L/S ratio of 0.34 ± 0.11. In this case the uncertainty arises mainly from the background in the sum spectrum.

The orbital polarization in $NiFe_2O_4$ can be compared with the values reported for other divalent nickel compounds. Fernandez *et al.*[29] measured an L/S ratio of 0.34 ± 0.06 for NiO using magnetic x-ray scattering. Arrio *et al.*[50] found an L/S ratio of ~0.25 for the molecular-based ferromagnetic $CsNiCr(CN)_6\cdot 2H_2O$ using XMCD. In our case, the line shape as well as the spin-orbit sum rule gives additional confirmation of the size of the orbital moment.

VIII. CONCLUSIONS

Most XMCD studies reported so far are only on ferromagnetic metals. The present study describes the application of this technique to ferrimagnetic oxides. These experiments open up new possibilities to study the magnetic properties of a class of strongly correlated materials which is still ill understood. The line shape of the XMCD spectrum of divalent nickel compounds is mainly determined by crystal-field and core-valence exchange interactions and it provides a relatively simple test case which can serve to understand more complicated systems.

We compared three different procedures, based on crystal-field theory and sum rules, to determine the L/S ratio at the nickel site of $NiFe_2O_4$. In the first method we performed a line shape fit of the XMCD by optimizing $10Dq$, which is the parameter for the octahedral crystal-field strength. This resulted in an L/S ratio of 0.27 for $10Dq = 1.2$ eV. In the second method we used the XMCD sum rules, which resulted in an L/S ratio of 0.27 ± 0.07. The sum rules offer the most general solution and require no *a priori* knowledge of the ground-state wave function. To account for *jj* mixing a correction factor of 0.93 was needed, which was derived with crystal-field theory. In the last method we determined the spin-orbit interaction using the sum rules for the isotropic spectrum. The spin-orbit value was corrected by a factor of 0.76 in order to take *jj* mixing into account. By converting the spin-orbit value into spin and orbital moment values using the crystal-field model, we obtained an L/S ratio of 0.34 ± 0.14. The agreement between the first two methods is good. This is, however, expected because if the curve fitting reproduces correctly the areas of the two absorption edges, the ground-state moments should match those obtained with the sum rules. Therefore, the agreement between the two methods cannot be interpreted as a proof that crystal-field theory gives a good description for the orbital magnetization. However, the crystal-field model predicts also correctly the XMCD line shape at the L_3 edge. There is a somewhat less perfect agreement for the L_2 edge, which can be ascribed to Coster-Kronig transitions.

Although the crystal-field model does not account for the effects such as hybridization and band structure, it provides a straightforward explanation for the orbital magnetization and, moreover, it confirms the validity of the interpretation of the spectra. Band-theory models often disregard spin-orbit interaction and, therefore, cannot account for the observed orbital magnetization. This can lead to an inaccurate description of magnetic properties such as the magnetocrystalline anisotropy and magnetostriction. The main deficiency of the calculation for the XMCD is not the omission of band-structure effects, but originates from the Coster-Kronig transitions between the discrete states with a $2p_{1/2}$ core hole and continuum states with a $2p_{3/2}$ core hole. This interaction causes a transfer of spectral weight in the magnetic dichroism signal near the onset of the L_2 edge. The Coster-Kronig process enhances the uncertainty in the integrated intensities and, hence, in the L/S ratio. It is, therefore, imperative to gain a deeper understanding of these processes by conducting further experiments and by performing calculations which take this effect explicitly into account.

ACKNOWLEDGMENTS

The XMCD project was funded under EPSRC Grant No. GR/L68568 in collaboration with Professor J. A. D. Matthew.

---

[1] C. T. Chen, Y. U. Idzerda, H. J. Lin, N. V. Smith, G. Meigs, E. Chaban, G. Ho, E. Pellegrin, and F. Sette, Phys. Rev. Lett. **75**, 152 (1995).

[2] H. Ebert, Rep. Prog. Phys. **59**, 1665 (1996).

[3] G. van der Laan, B. T. Thole, G. A. Sawatzky, J. B. Goedkoop, J. C. Fuggle, J. M. Esteva, R. C. Karnatak, J. P. Remeika, and H. A. Dabkowska, Phys. Rev. B **34**, 6529 (1986).

[4] F. Sette, C. T. Chen, Y. Ma, S. Modesti, and N. V. Smith, in *X-Ray and Inner-Shell Processes*, edited by T. A. Carlson, M. O. Krause, and S. T. Manson, AIP Conf. Proc. No. 215 (AIP, New York, 1990), 787.

[5] W. F. Pong, Y. K. Chang, M. H. Su, P. K. Tseng, H. J. Lin, G. H. Ho, K. L. Tsang, and C. T. Chen, Phys. Rev. B **55**, 11 409 (1997).

[6] P. Kuiper, B. G. Searle, L. C. Duda, R. M. Wolf, and P. J. van der Zaag, J. Electron Spectrosc. Relat. Phenom. **86**, 107 (1997).

[7] G. van der Laan and B. T. Thole, Phys. Rev. B **43**, 13 401 (1991).

[8] H. J. de Boer and E. J. W. Verwey, Proc. Phys. Soc. London **49**, 59 (1937).

[9] F. Bloch, Z. Phys. **57**, 545 (1929).

[10] A. H. Wilson, Proc. Phys. Soc. London **133**, 458 (1931).

[11] L. F. Mattheiss, Phys. Rev. B **5**, 306 (1972).

[12] N. F. Mott, Proc. Phys. Soc. London, Sect. A **62**, 416 (1949).

[13] J. Hubbard, Proc. Phys. Soc. London **277**, 237 (1964); **281**, 401 (1964).

[14] J. Zaanen, G. A. Sawatzky, and J. W. Allen, Phys. Rev. Lett. **55**, 418 (1985).

[15] G. van der Laan, R. A. D. Pattrick, C. M. B. Henderson, and D. J. Vaughan, J. Phys. Chem. Solids **53**, 1185 (1992).

[16] G. van der Laan, C. Westra, C. Haas, and G. A. Sawatzky, Phys. Rev. B **23**, 4369 (1981).

[17] A. Fujimori and F. Minami, Phys. Rev. B **30**, 957 (1984).

[18] G. A. Sawatzky and J. W. Allen, Phys. Rev. Lett. **53**, 2339 (1984).

[19] J. M. McKay and V. E. Henrich, Phys. Rev. Lett. **53**, 2343 (1984).

[20] K. Terakura, A. R. Williams, T. Oguchi, and J. Kübler, Phys. Rev. Lett. **52**, 1830 (1984); K. Terakura, T. Oguchi, A. R. Williams, and J. Kübler, Phys. Rev. B **30**, 4734 (1984).

[21] C. H. La Blanchetais, J. Phys. Radium **12**, 765 (1951).

[22] C. G. Schull, W. A. Strauser, and E. O. Wollon, Phys. Rev. **83**, 353 (1951).

[23] M. D. Towler, N. L. Allen, N. M. Harrison, V. R. Saunders, W. C. Mackrodt, and E. Aprà, Phys. Rev. B **50**, 5041 (1994).

[24] G. J. M. Janssen and W. C. Nieuwpoort, Phys. Rev. B **38**, 3449 (1988).

[25] D. J. Dunlop and Ö. Özdemir, *Rock Magnetism: Fundamentals and Frontiers* (Cambridge University Press, New York, 1997).

[26] M. Pénicaud, B. Siberchicot, C. B. Sommers, and J. Kübler, J. Magn. Magn. Mater. **103**, 212 (1992).

[27] J. Kanamori, Prog. Theor. Phys. **17**, 197 (1957).

[28] A. Svane and O. Gunnarsson, Phys. Rev. Lett. **65**, 1148 (1990).

[29] V. Fernandez, C. Vettier, F. de Bergevin, C. Giles, and W. Neubeck, Phys. Rev. B **57**, 7870 (1998).

[30] L. Severin, M. S. S. Brooks, and B. Johansson, Phys. Rev. Lett. **71**, 3214 (1993).

[31] I. V. Solovyev, A. I. Liechtenstein, and K. Terakura, J. Magn. Magn. Mater. **185**, 118 (1998).

[32] G. van der Laan and B. T. Thole, Phys. Rev. B **42**, 6670 (1990).

[33] G. van der Laan and B. T. Thole, Phys. Rev. B **43**, 13 401 (1991).

[34] G. van der Laan, J. Zaanen, G. A. Sawatzky, R. Karnatak, and J. M. Esteva, Phys. Rev. B **33**, 4253 (1986).

[35] G. van der Laan, B. T. Thole, G. A. Sawatzky, and M. Verdaguer, Phys. Rev. B **37**, 6587 (1988).

[36] G. van der Laan and B. T. Thole, Phys. Rev. Lett. **60**, 1977 (1988).

[37] A. Tanaka and T. Jo, J. Phys. Soc. Jpn. **63**, 2788 (1992).

[38] A. Kotani and K. Okada in *Recent Advances in Magnetism of Transition Metal Compounds*, edited by A. Kotani and N. Suzuki (World Scientific, Singapore, 1993).

[39] M. Lenglet, A. D'Huysser, J. P. Bonnelle, J. Dürr, and C. K. Jørgensen, Chem. Phys. Lett. **136**, 478 (1987).

[40] M. Lenglet, F. Hochu, J. Dürr, and M. H. Tuilier, Solid State Commun. **104**, 793 (1997).

[41] G. van der Laan, C. S. Mythen, and H. A. Padmore, Europhys. Lett. **11**, 67 (1990).

[42] G. van der Laan, Phys. Rev. B **51**, 240 (1995).

[43] G. van der Laan, J. Phys.: Condens. Matter **10**, 3239 (1998).

[44] R. D. Cowan, *The Theory of Atomic Structure and Spectra* (University of California Press, Berkeley, 1981).

[45] P. H. Butler, *Point Group Symmetry, Applications, Methods and Tables* (Plenum, New York, 1981).

[46] B. T. Thole, P. Carra, F. Sette, and G. van der Laan, Phys. Rev. Lett. **68**, 1943 (1992).

[47] G. van der Laan, Phys. Rev. B **57**, 112 (1998).

[48] P. Carra, B. T. Thole, M. Altarelli, and X. Wang, Phys. Rev. Lett. **70**, 694 (1993).

[49] B. T. Thole and G. van der Laan, Phys. Rev. B **38**, 3158 (1988); Phys. Rev. A **38**, 1943 (1988).

[50] M.-A. Arrio, Ph. Sainctavit, Ch. Cartier dit Moulit, Ch. Brouder, F. M. F. de Groot, T. Mallah, and M. Verdaguer, Nucl. Instrum. Methods Phys. Res. B **97**, 453 (1995).